Impact of land surface processes on the South American warm season climate

**H.-Y. Ma · C. R. Mechoso · Y. Xue · H. Xiao ·
C.-M. Wu · J.-L. Li · F. De Sales**

Abstract The present study demonstrates that (1) the simulation of the South American warm season (December–February) climate by an atmospheric general circulation model (AGCM) is sensitive to the representation of land surface processes, (2) the sensitivity is not confined to the "hot spot" in Amazonia, and (3) upgrading the representation of those processes can produce a significant improvement in AGCM performance. The reasons for sensitivity and higher success are investigated based on comparisons between observational datasets and simulations by the AGCM coupled to either a simple land scheme that specifies soil moisture availability or to the Simplified Simple Biosphere Model (SSiB) that allows for consideration of soil and vegetation biophysical process. The context for the study is the UCLA AGCM. The most notable simulation improvements are along the lee of the Andes in the lower troposphere, where poleward flow transports abundant moisture from the Amazon basin to high latitudes, and in the monsoon region where the intensity and pattern of precipitation and upper level ice water content are more realistic. It is argued that a better depiction of the Chaco Low, which is controlled by local effects of land surface processes, decisively contributes to the superior model performance with low-level flows in central South America. The better representation of the atmospheric column static stability and large-scale moisture convergence in tropical South America contribute to more realistic precipitation over the monsoon region. The overall simulation improvement is, therefore, due to a combination of different regional processes. This finding is supported by idealized AGCM experiments.

Keywords Land surface processes · AGCM · South American monsoon · SACZ · Chaco Low

1 Introduction

Precipitation changes over South America projected in different climate change scenarios by climate models participating in the Intergovernmental Panel on Climate Change Fourth Assessment Report (IPCC AR4, IPCC 2007) show large spread both in sign and magnitude (Fig. 3.3 of the report). The different ways in which climate models represent land surface processes and associated sensitivity to changes in land surface conditions is one of the principal contributions to this spread (e.g. Marengo et al. 2003; Koster et al. 2004; Dirmeyer et al. 2006, 2009). Zeng and Neelin (1999) working in a simple theoretical framework suggested that sensitivity of precipitation over land to underlying surface conditions depends on different nonlinear processes, such as cloud radiative and evaporation feedbacks. The importance of these processes, in turn, strongly depends on the background state, i.e., the model's climatology. Therefore, a realistic model climatology is crucial prerequisite for reliable climate projections. The present study demonstrates that different representations of land surface processes in an atmospheric general circulation model (AGCM) can

H.-Y. Ma (✉) · C. R. Mechoso · Y. Xue · H. Xiao · C.-M. Wu
Department of Atmospheric and Oceanic Sciences,
University of California Los Angeles, Los Angeles, CA, USA
e-mail: hyma@atmos.ucla.edu

Y. Xue · F. De Sales
Department of Geography, University of California Los Angeles,
Los Angeles, CA, USA

J.-L. Li
Jet Propulsion Laboratory, California Institute of Technology,
Pasadena, CA, USA

result in significantly different simulations of South American warm season climate. In our case, the most comprehensive parameterization of land surface processes we use obtains the most successful of the two simulations.

The South American Monsoon System (SAMS) is a key feature of the warm season (December–February) climate over South America. SAMS starts developing during the southern spring when intense convection shifts rapidly from northwestern South America to the southern Amazon Basin and Brazilian Highlands (Nogués–Paegle et al. 2002; Mechoso et al. 2004; Vera et al. 2006a, b). The upper-level Bolivian high—Nordeste trough system becomes firmly established during mid-summer. The low-level circulation transports moisture westward from the tropical Atlantic to the Amazon basin, and then southeastward toward the extra-tropics into the Chaco Low region. Near the eastern slopes of the Andes Mountains, the monsoon circulation includes the South American low-level jet (SALLJ) (Byerle and Paegle 2002; Campetella and Vera 2002). Another outstanding component of SAMS is the South American Convergence Zone (SACZ, Kodama 1992), which extends southeastward from Amazonia over the Atlantic Ocean. SAMS starts decaying in February, and continues to weaken throughout the southern fall as convection gradually retreats toward the equator. Additional details on SAMS climatology are provided in Nogués–Paegle et al. (2002), Mechoso et al. (2004), Vera et al. (2006a, b), and references therein.

Several modeling studies on SAMS have been made with AGCMs. On the basis of idealized AGCM experiments, Lenters and Cook (1995) find that the summer precipitation maxima in the Amazon, SACZ, and northwestern South America can be obtained with zonally uniform SSTs and without topographic elevations; realistic topography improves the position and strength of precipitation of those features. Zhou and Lau (2002) compare the SAMS climatology simulated by six AGCMs. The models capture major features of SAMS, such as SACZ and low-level circulations. The magnitude of the Atlantic subtropical high and Chaco Low, however, tends to be overestimated. The too intense Chaco Low is associated with a too strong southerly flow along the Andes. Large rainfall errors around the Andes and SACZ extension over the western Atlantic are indicative of the AGCMs difficulties with the representation of steep mountains and convective processes. Meehl et al. (2006) show that some AGCMs tend to underestimate precipitation in northern coastal Brazil and French Guiana, and attribute such a feature to insufficient model resolution. Vera et al. (2006a, b) find in seven World Climate Research Programme's phase three of coupled model intercomparison project (WCRP-CMIP3) models increased precipitation over the northern Andes and southeastern South America and decreased precipitation along the southern Andes in the period of 2070–2099 relative to 1970–1999. In central Amazonia, there is no consensus in sign changes of precipitation projections. Lin et al. (2009) evaluate the intraseasonal variability of summer precipitation over South America in 14 WCRP-CMIP3 coupled GCMs: most of these models underestimate seasonal mean precipitation over SAMS region and all models underestimate the total intraseasonal variability. Bombardi and Carvalho (2009) also examine the SAMS variability as well as the onset, end, and total rainfall during southern summer in WCRP-CMIP3 coupled models. According to their results, most models misrepresent the ITCZ and therefore do not capture the actual annual cycle of precipitation over the Amazon and northwest South America for the period of 1981–2000. They also find that the most coherent feature observed in the models for the A1B scenario is a reduction in precipitation over central-eastern Brazil during the southern summer for the period of 2081–2100. The models, however, do not produce statistically significant changes in SAMS onset and demise dates.

To illustrate the performance of contemporary AGCMs on SAMS simulations we present in Fig. 1 the mean warm season (December–February mean) precipitation over South America for the period 1979–2000 as obtained from the Atmospheric Model Intercomparison Project (AMIP) experiment from the WCRP-CMIP3 multi-model datasets (see Table 1 for a list of models). Figure 1 also displays precipitation distributions from the Daily Precipitation Grid for South America (SA19, Liebmann and Allured 2005), Climate Prediction Center merged analysis of precipitation (CMAP, Xie and Arkin 1997), and Tropical Rain Measuring Mission (TRMM, Kummerow et al. 2000). The mean precipitation pattern from observational datasets shows a center of intense precipitation in central Amazonia with a highest value of around 11 mm day^{-1}. TRMM and CMAP depict the SACZ with values between 6 to 8 mm day^{-1}. All the WCRP-CMIP3 AGCMs reproduce the main features of SAMS to some extent. There are, however, significant errors and inter-model differences. Most simulations underestimate precipitation in central Amazonia, except for HADGEM1, NCAR-PCM1, high resolution MICRO32, and CNRM-CM3. Moreover, these uncoupled models either underestimate or even fail to reproduce the SACZ as reported in previous analysis of WCRP-CMIP3 coupled models (e.g. Vera et al. 2006a, b, 20C3M).

It is well known that land surface processes affect the atmosphere through exchanges of energy and water in the planetary boundary layer (PBL), which ultimately affect the large-scale flow, precipitation and cloudiness. Many studies with numerical models have documented a positive feedback between soil moisture and precipitation
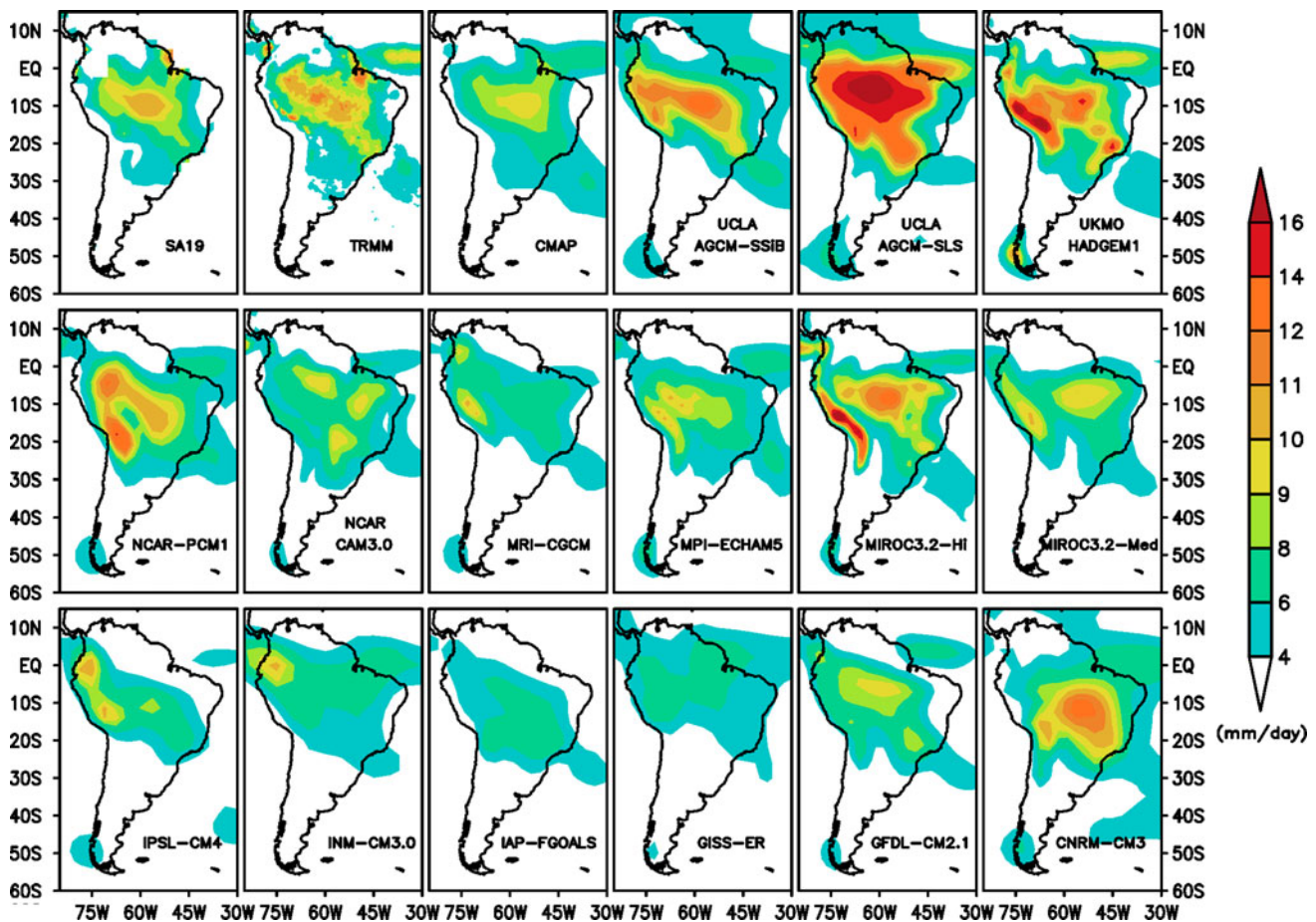
Fig. 1 December–February mean precipitation (mm day^{-1}) from daily precipitation grid for South America (SA19), TRMM, CMAP, and model simulations from uncoupled UCLA AGCM with simple land scheme (AGCM/SLS), coupled UCLA AGCM-SSiB (AGCM/LSM), and AMIP experiments from WCRP-CMIP3 multi-model datasets. See Table 1 for the list of models

(e.g. Mintz 1984; Beljaars et al. 1996; Pal and Eltahir 2001; Collini et al. 2008). Accordingly, precipitation leads to enhanced soil moisture and further increases in rainfall. For example, Collini et al. (2008) investigate the sensitivity of SAMS to initial conditions in soil moisture by performing one-month long runs with a regional mesoscale model. They find that precipitation is more sensitive to initial reductions of soil moisture than to increases, and discuss mechanisms of positive feedback. In one mechanism, the soil moisture reduction leads to smaller latent heat flux and larger sensible heat flux. These two effects lead to a drier and warmer boundary layer, which in turn reduces the atmospheric instability. Further, the deeper (and drier) boundary layer is related to a stronger and higher South American low-level jet (SALLJ), which transports less moisture since the atmosphere is drier. The combination of reduced convective instability and reduced moisture flux convergence act concurrently to diminish the precipitation in the SAMS core. For this region, Grimm et al. (2007) argue that peak precipitation is negatively correlated with soil moisture in the antecedent spring season. Vegetation

biophysical processes can also affect the energy and water fluxes over land surfaces. From results of AGCM experiments, Xue et al. (2006) propose that including both explicit vegetation and soil processes results in more successful simulations of SAMS than when only the latter process are taken into account. According to their results, consideration of vegetation process produces more realistic values of the surface Bowen ratio (i.e., the ratio of sensible to latent heat flux), which affects the large-scale circulation and precipitation.

The present study shows that an improved simulation of SAMS climatological precipitation and circulations can be obtained by upgrading land surface processes in the UCLA AGCM without any other model change. The reasons for improvement are investigated. Our approach uses both observational and reanalysis datasets, and simulations by the AGCM. The remainder of the text is organized into five sections. Section 2 provides a brief introduction to the observational and reanalysis datasets, and models used in this study. Section 3 discusses the impact of land surface processes on the simulated warm season climate of South

Table 1 List of selected models, and their originating groups and countries of the Atmospheric Model Intercomparison Project (AMIP) experiment from the Intergovernmental Panel on Climate Change 4th assessment report (IPCC AR4), now known as the WRCP-CMIP3 multi-model datasets

Model ID	Originating group(s)	Country
CNRM-CM3	Météo-France/Center National de Recherches Météorologiques	France
GFDL-CM2.1	US Department of Commerce/NOAA/Geophysical Fluid Dynamics Laboratory	USA
GISS-ER	NASA/Goddard Institute for Space Studies	USA
FGOALS	LASG/Institute of Atmospheric Physics	China
INM-CM3.0	Institute for Numerical Mathematics	Russia
IPSL-CM4	Institut Pierre Simon Laplace	France
MIROC3.2(medres)	Center for Climate System Research (The University of Tokyo), National Institute for Environmental Studies, and Frontier Research Center for Global Change (JAMSTEC)	Japan
MIROC3.2(hires)	Center for Climate System Research (The University of Tokyo), National Institute for Environmental Studies, and Frontier Research Center for Global Change (JAMSTEC)	Japan
ECHAM5/MPI-OM	Max Planck Institute for Meteorology	Germany
MRI-CGCM	Meteorological Research Institute	Japan
CAM3.0	National Center for Atmospheric Research	USA
PCM1	National Center for Atmospheric Research	USA
UKMO-HadGEM1	Hadley Center for Climate Prediction and Research/Met Office	UK

Refer the following website for more detailed description of the models: http://www-pcmdi.llnl.gov/ipcc/model_documentation/ipcc_model_documentation.php

America, and Sect. 4 examines the mechanisms for regional impact. Section 5 presents a summary and our conclusions.

2 Datasets and models

2.1 Reanalysis and observational datasets

We use global datasets from European center for medium-range weather forecasts (ECMWF) ERA40 (Uppala et al. 2005). The ERA40 covers the period from mid-1957 to 2001 and its high vertical coverage up to 1 mb allows for plotting vertical cross section of large-scale heat and moisture budget residuals (Yanai et al. 1973) suitable for AGCM verification. Although the widely usage and well recognition of this dataset, caution should be exercised since some problems of this dataset regarding the region of interest, such as cold bias of temperature, and low bias in precipitation over the Amazon were reported in previous study (Betts et al. 2005; Fernandes et al. 2008).

We also use several observational datasets including SA19, CMAP, TRMM and CloudSat (Stephens et al. 2008; and Woods et al. 2008). The CMAP data consists of monthly analyses of global precipitation, in which observations from raingauges are merged with precipitation estimates from several satellite-based algorithms (infrared and microwave). The coverage period for CMAP in this study is from 1979 to 2006. SA19 is based on information provided by approximately 7,900 South American meteorological stations during the period 1940 to mid-2006, and is synthesized into daily fields. The TRMM and CloudSat are both NASA's satellite missions for rainfall and clouds observation. The retrieval algorithm for TRMM is 3B42 with 3-hourly temporal resolution, and covers from November 1997 to the present date. Followed Waliser et al.(2009), CloudSat RO4 (Stephens et al. 2008) ice water content (IWC) filtered out retrievals that were associated with convective cloud types (using CloudSat cloud classification) or that were flagged as exhibiting surface precipitation are used for model-data comparison (details referred to Woods et al. 2008; Waliser et al. 2009). The product for CloudSat covers from June 2006 to the present date.

2.2 Atmospheric model: UCLA AGCM

The University of California Los Angeles (UCLA) AGCM includes advanced parameterizations of the major physical processes in the atmosphere. The parameterization of cumulus convection, including its interaction with the planetary boundary layer (PBL), follows the prognostic version of Arakawa and Schubert (1974) presented by Pan and Randall (1998). The parameterization of radiative processes is based on Harshvardhan et al. (1987, 1989), and the parameterization of PBL processes is based on the

mixed-layer approach of Suarez et al. (1983), as revised by Li et al. (2002). Surface heat fluxes are calculated following the bulk formula proposed by Deardorff (1972) and modified by Suarez et al. (1983). The model also includes the parameterizations of prognostic cloud liquid water and ice (Köhler 1999), and the impact of cumulus cloud fraction on radiative calculations. A more detailed AGCM description is given in Arakawa (2000) and Mechoso et al. (2000), or online at http://www.atmos.ucla.edu/~mechoso/esm/agcm.html.

In the present study, we use model version 7.1 with a horizontal resolution of 2.5° latitude and 2° longitude, and 29 vertical levels. The distributions of green house gases, sea ice, SST, surface albedo, surface roughness, and ground wetness are all prescribed corresponding to a monthly varying climatology.

2.3 Land surface models

The AGCM incorporates a simple land surface scheme for prediction of ground temperature over land. The algorithm is based on energy balance of net surface shortwave radiation, net surface longwave radiation, sensible heat, and latent heat fluxes. The distribution of potential evaporation for the calculation of surface evaporation is prescribed based on observational data and adjustments according to model results ("tuning").

As an alternative for the simple land component, the AGCM incorporates the first generation of the Simplified Simple Biosphere Model (SSiB; Xue et al. 1991). This version of SSiB has three soil layers and one vegetation layer. Soil moisture of the three soil layers, interception water store for the canopy, deep soil temperature, ground temperature, and canopy temperature are predicted based on the water and energy balance at canopy and soil. Three aerodynamic resistances are introduced to control the heat and water fluxes between the canopy layer air space and (1) canopy leaves, (2) soil surface, and (3) the reference PBL height. The values of these resistances are determined in terms of vegetation properties, ground conditions and bulk Richardson number based on the Monin–Obukhov similarity theory (Paulson 1970; Businger et al. 1971; Deardorff 1972; Sellers et al. 1986; Xue et al. 1991; 1996a). The surface albedo has diurnal variations based on the change of net solar radiation in the canopy layer due to vegetation properties. Several data sources (Dorman and Sellers, 1989; Xue et al. 1996b) have been used to determine the vegetation types that specify monthly climatological land surface properties (e.g., leaf area index, green leaf fraction and surface roughness length).

SSiB provides the AGCM with *momentum, sensible and latent heat fluxes*, *radiative skin temperature* (ground temperature in the AGCM with the simple scheme), and *surface albedo*. The AGCM provides SSiB with *terrain pressure, precipitation, incoming short wave and long wave radiative fluxes at surface*, and *solar zenith angle*, as well as *pressure, velocity, moisture*, and *temperature* in the PBL. The land scheme is treated as another component of the AGCM, for which the time step is 1 h in the present study.

2.4 Experimental design and overview of AGCM performance

To assess our AGCM's ability to represent the mean climate, we examine results of two 30-year long simulations using monthly-varying SST from the climatology compiled by Reynolds and Smith (1995). One is a control simulation using the simple land scheme (AGCM/SLS hereafter); the other simulation is made with the AGCM coupled to the SSiB land surface model (AGCM/LSM hereafter). The initial conditions were taken from a previous, multi-year model run starting from 1 October 1982 (see Köhler 1999).

We start by comparing the December–February mean sea level pressure (SLP) from the ERA40 Reanalysis (Fig. 2a) and the simulations (Fig. 2b, c). The overall features of the field are well captured in the outputs. The unrealistically low values in the Himalayan and Andes regions are artifacts of the numerical extrapolation in the presence of steep terrain (Köhler 1999). The two simulations produce qualitatively similar results, but there are clear regional differences. For example, in AGCM/LSM, the subtropical highs in the Southern Pacific, Southern Atlantic and Indian Oceans are slightly better captured than in AGCM/SLS.

Figure 3 shows annual mean precipitation from the CMAP dataset (Fig. 3a) and the simulations (Fig. 3b, c). Both simulations capture the outstanding features of the global precipitation distributions: ITCZ, South Pacific Convergence Zone (SPCZ), SACZ, main monsoon, and extratropical storm tracks. The global mean values from the simulations (3.6 mm day^{-1} for AGCM/SLS and 3.4 mm day^{-1} for AGCM/LSM) are substantially larger than in CMAP (2.7 mm day^{-1}); surface evaporation is also too high in the simulations (not shown here). A comparison between precipitation in AGCM/SLS and AGCM/LSM clearly shows that the latter obtains a more realistic pattern, in which the positive biases observed in the former are reduced over most land areas. Xue et al. (2010) report a similar result and indicate that including vegetation biophysical processes also results in more realistic values of the simulated Bowen ratio.

We next narrow down on South America and compare the simulated December–February mean precipitation with the corresponding distributions in SA19, TRMM,
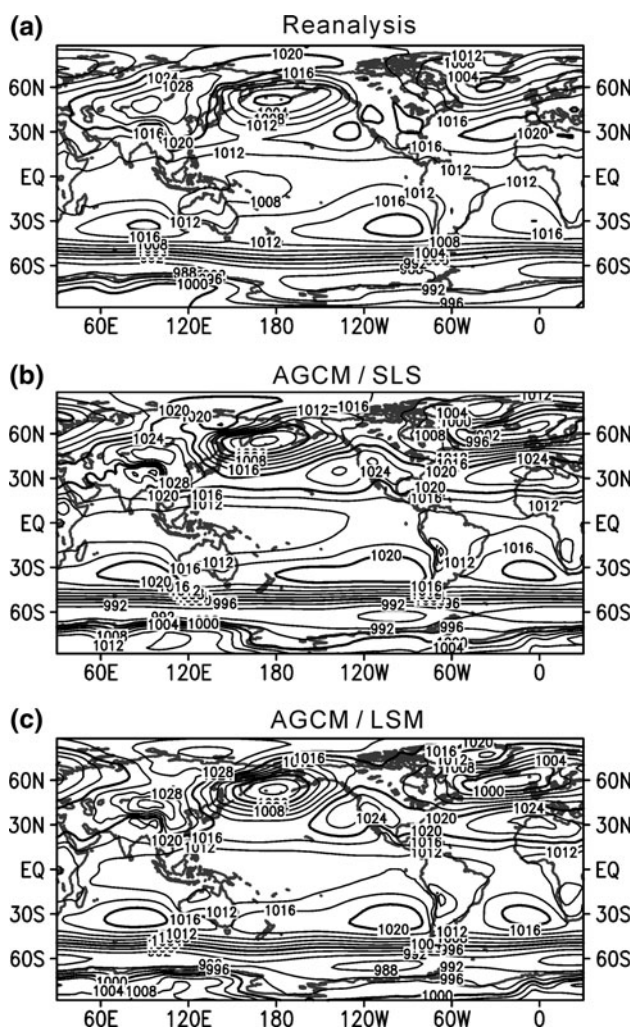
Fig. 2 December–February mean sea level pressure in (mb) from
a ERA40 Reanalysis, b uncoupled UCLA AGCM with simple land
scheme (AGCM/SLS), and c coupled UCLA AGCM-SSiB (AGCM/
LSM)

Fig. 3 December–February mean precipitation in (mm day^{-1}) from
a CMAP (2.7 mm day^{-1}), b uncoupled UCLA AGCM with simple
land scheme (AGCM/SLS) (3.6 mm day^{-1}), and c coupled UCLA
AGCM-SSiB (AGCM/LSM) (3.4 mm day^{-1}). The values in the
parentheses are the global mean precipitation

and CMAP (Fig. 1). We also contrast our results with those
from the AMIP models. Both simulations capture most of
the main features in the precipitation field, except for the
too high values in central Amazonia. AGCM/LSM is more
successful in reproducing the observed precipitation pat-
tern than AGCM/SLS, and arguably than the most suc-
cessful AMIP model. The strong overestimation of
precipitation over the Amazon basin in AGCM/SLS is
significantly reduced in AGCM/LSM. The location
and intensity of SACZ is also better simulated in the latter
run.

The results demonstrate state-of-the-art performance of
both AGCM/SLS and AGCM/LSM, albeit intensity pre-
cipitation is on the high side even considering the uncer-
tainty of observational estimates. We concentrate on the
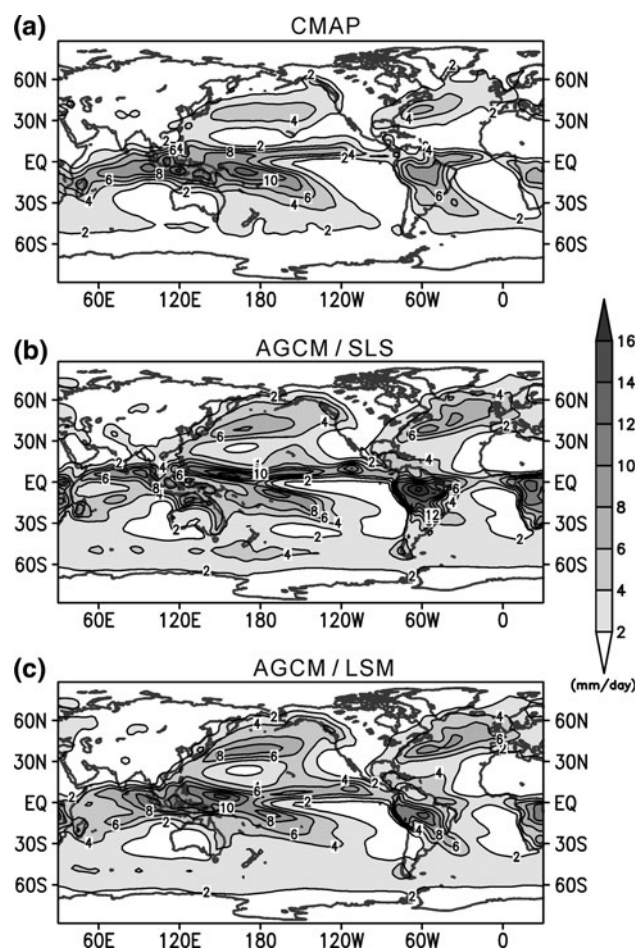simulated South American climate in the remainder of this
paper.

3 Impact of land surface processes on the South American climate

3.1 Impact on heat and moisture fluxes

Figure 4 shows the December–February mean differences
between AGCM/LSM and AGCM/SLS in surface sensible
heat flux (Fig. 4a), surface evaporation (Fig. 4b), precipi-
tation (Fig. 4c), vertically integrated moisture flux con-
vergence (Fig. 4d), total cloud cover (Fig. 4e), surface
albedo (Fig. 4f), and net longwave and shortwave fluxes at
surface (Fig. 4g, h). Regions where differences are statis-
tically significant at the 95% confidence level are shaded.
AGCM/LSM obtains significantly higher sensible heat flux
and lower surface evaporation (or latent heat flux with the
conversion of latent heat of vaporization) than AGCM/
SLS, mostly in southern South America. There are three
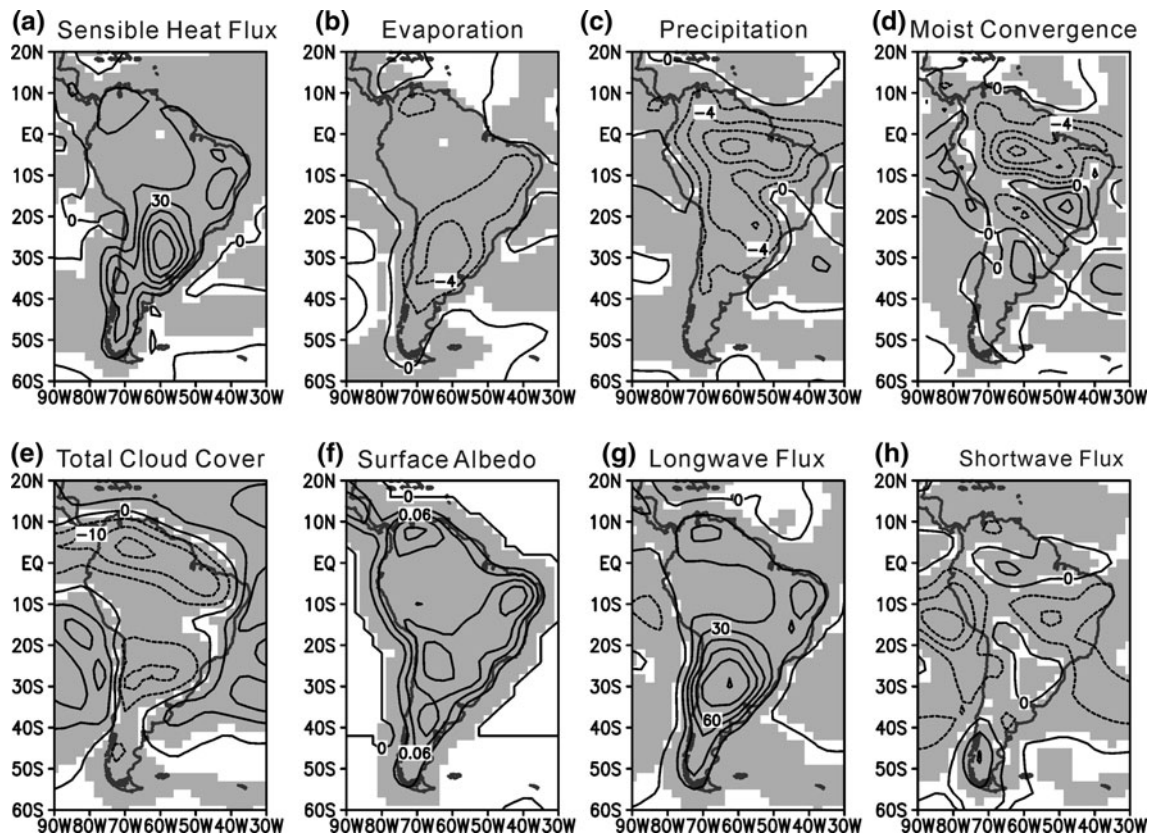local maxima of sensible heat flux located around 70°W,

Fig. 4 Difference of December–February mean **a** surface sensible heat flux (contour interval is 15 W m^{-2}), **b** surface evaporation (contour interval is 2 mm day^{-1}), **c** precipitation (contour interval is 2 mm day^{-1}), **d** vertically integrated moisture flux convergence (contour interval is 2 mm day^{-1}), **e** total cloud cover (contour interval is 10%), **f** surface albedo (contour interval is 0.03), **g** net surface longwave flux (contour interval is 15 W m^{-2}), and **h** net surface shortwave flux (contour interval is 15 W m^{-2}), between coupled UCLA AGCM-SSiB (AGCM/LSM) and uncoupled UCLA AGCM with simple land scheme (AGCM/SLS). Regions where differences are statistically significant at the 95% confidence level are shaded

60°W and 45°W. A study with the NCEP GCM has suggested that the sensible heat fluxes over the savanna and shrub lands over that area have important impact on the SAMS moisture flow (Xue et al., 2006). A similar feature is found in the present study, as shown later in Sect. 3.3. The precipitation is significantly weaker over most tropical and sub-tropical South America, which suggests weaker convection in those regions. The SACZ region, however, shows stronger precipitation. The pattern of precipitation differences is consistent with that of vertically integrated moisture flux convergence and total cloud cover. In general, the surface albedo is slightly larger all over the continent, consistent with the findings of Xue et al. (2010). The net surface longwave radiation is higher due to increased ground temperature (not shown here). The net surface shortwave radiation is affected by both the surface albedo and cloud cover. Lower cloud cover is consistent with increased incoming short wave radiation, but higher surface albedo reflects more shortwave radiation to the atmosphere. In this case, the cloud cover effect is larger since the regions with positive differences are mostly

positively correlated with regions with lesser cloud cover. The overall AGCM response to the upgraded representation of land surface processes agrees with the conceptual analysis by Zeng and Neelin (1999) for the tropical deforestation problem.

In the following sub sections, we focus on the impact land surface processes on the simulated precipitation and low level circulations.

3.2 Impact on precipitation in central Amazonia

To gain quantitative insight on the relationship between weaker precipitation in AGCM/LSM and accompanying changes in surface energy and water fluxes, we examine the large-scale heat and moisture budget residuals represented by the apparent heat source Q_1 and apparent moisture sink Q_2 (Yanai et al. 1973; Hung 2003). These residuals are defined by the following expressions:

$$Q_1 \equiv c_p \left(\frac{p}{p_0}\right)^{\kappa} \left(\frac{\partial \bar{\theta}}{\partial t} + \bar{\mathbf{v}} \nabla \bar{\theta} + \bar{\omega} \frac{\partial \bar{\theta}}{\partial p}\right) \tag{1}$$

$$Q_2 \equiv -L\left(\frac{\partial \bar{q}}{\partial t} + \bar{\mathbf{v}}\nabla \bar{q} + \bar{\omega}\frac{\partial \bar{q}}{\partial p}\right) \qquad (2)$$

where θ is the potential temperature, q is mixing ratio, $\bar{\mathbf{v}}$ is horizontal velocity, ω is vertical velocity in the pressure coordinate, L latent heat of vaporization, $\kappa = Rc_p^{-1}$ with R being the gas constant and c_p the specific heat capacity of dry air at constant pressure, and $p_0 = 1,000$ mb. Overbars represent the running horizontal average over a large-scale area. The expressions for Q_1 and Q_2 can also be rewritten as

$$Q_1 \equiv Q_R + L(\bar{c} - \bar{e}) - \nabla\overline{s'\mathbf{v}'} - \frac{\partial \overline{s'\omega'}}{\partial p} \qquad (3)$$

$$Q_2 \equiv L(\bar{c} - \bar{e}) - \nabla\overline{q'\mathbf{v}'} - \frac{\partial \overline{q'\omega'}}{\partial p} \qquad (4)$$

where Q_R is the radiative heating rate, c and e are condensation and evaporation per unit mass of air, respectively, and s is dry static energy. The primes represent the deviation from the average indicated by the overbars. The terms on the right hand side of Eq (3) represent, therefore, the total effect of radiative heating, latent heat released by net condensation, and horizontal and vertical convergence of sensible heat fluxes due to sub-grid scale eddies, such as cumulus convection and turbulence. The terms on the right hand side of Eq (4) represent the total effect of net condensation, and divergence of eddy moisture flux due to sub-grid scale eddies.

Figure 5 shows latitude-height sections of December–February mean Q_1 (top three panels) and Q_2 (bottom three panels) zonally averaged between 70°W and 50°W (contours), as well as their standard deviation (shaded) for the ERA40 Reanalysis and the simulations. The units have been converted into (K day^{-1}) by multiplying c_p^{-1}. In central Amazonia, the Q$_1$ profile from ERA40 shows a strong heating center around 500 mb, with largest values between 5°S and 15°S. Q$_1$ from AGCM/SLS and AGCM/LSM have similar vertical structure, except that the maximum center is shifted by 2–4°. The Q_2 profile from ERA40 in central Amazonia has a similar structure to that of Q_1. The corresponding Q_2 profiles from AGCM/SLS and AGCM/LSM are also similar, except that maximum values are around the 700 mb level, which is below the level of maximum Q_1. This profile structure of Q_1 and Q_2 indicates
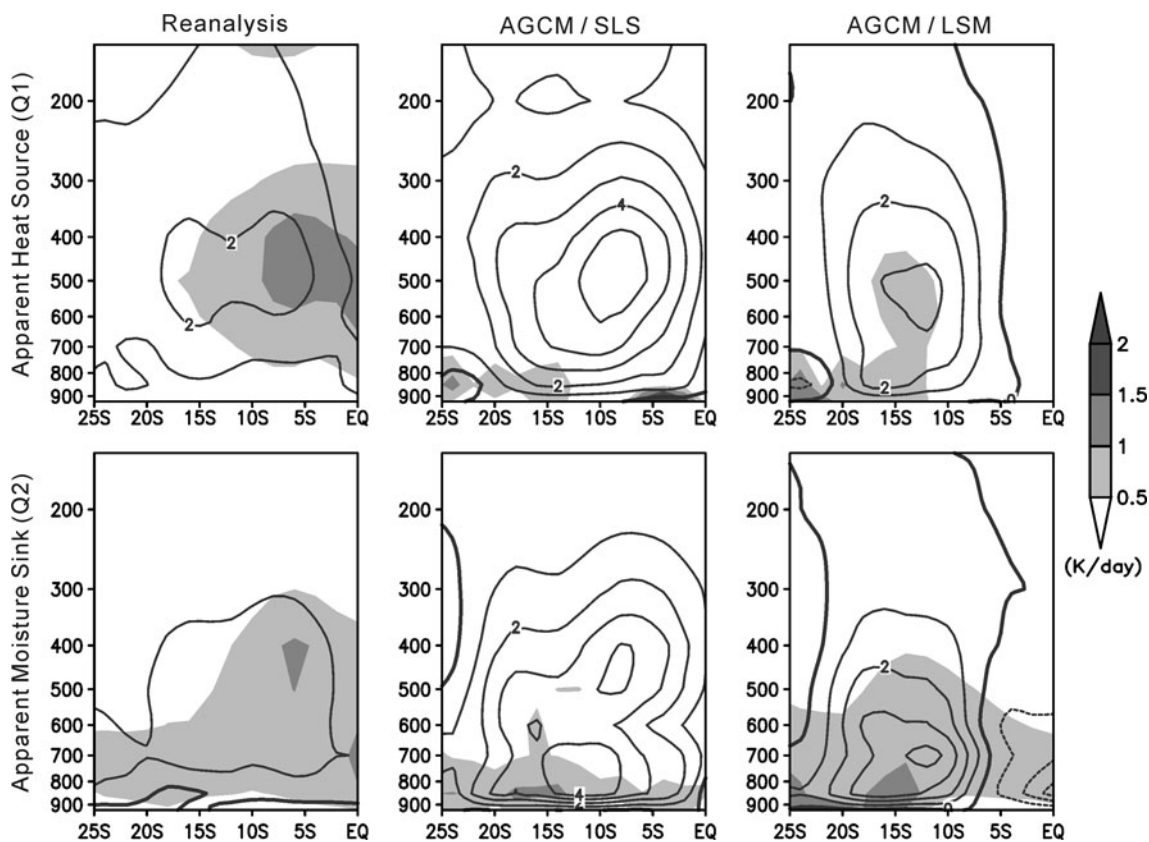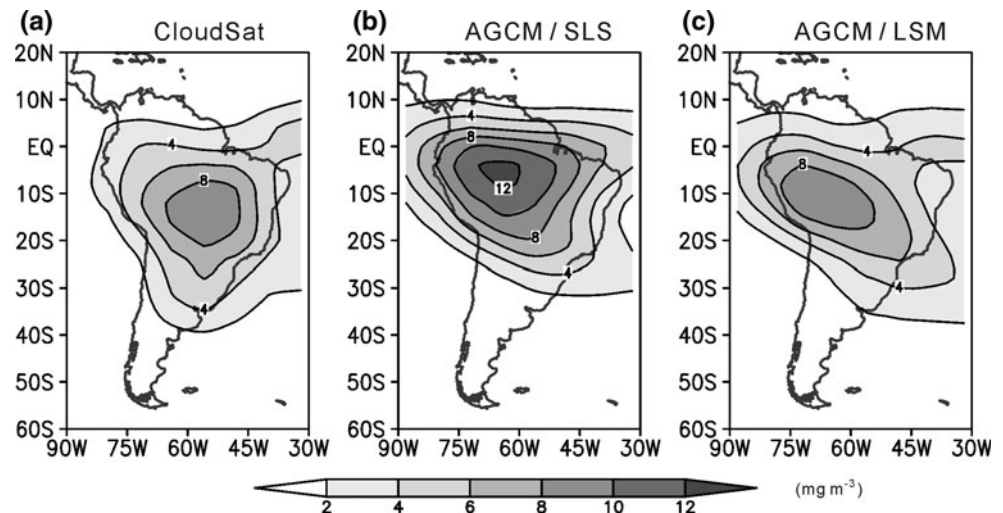

Fig. 5 Latitude-height (mb) sections of the December–February mean apparent heat source (upper row) and moisture sink (lower row) averaged over 70°W–50°W from ERA40 Reanalysis (Left), uncoupled UCLA AGCM with simple land scheme (AGCM/SLS) (middle), and coupled UCLA AGCM-SSiB (AGCM/LSM) (right). Contour interval is 1 (K day^{-1}). Also plotted in shade is the standard deviation

Fig. 6 December–February mean cloud ice water content (IWC; mg m^{-3}) at 215 mb from **a** CloudSat estimates of mean IWC (mg m^{-3}) filtered out retrievals with precipitation detected at the surface and retrievals identified with convective clouds (i.e., non-precipitating and non-convective; referred to as NPC), **b** uncoupled UCLA AGCM with simple land scheme (AGCM/SLS), **c** coupled UCLA AGCM-SSiB (AGCM/LSM). Contour is 2 (mg m^{-3})

a dominant contribution of heating by condensation processes due to convective activity (e.g., Luo and Yanai 1984; Yanai and Tomita 1998). The magnitude of the heating represented by Q_1 in central Amazonia from AGCM/LSM is significantly weaker than that from AGCM/SLS, and thus is closer to the ERA40 values. The heating due to saturation condensation from the Q_2 profile is also weaker in the lower troposphere, which also suggests a dryer lower troposphere and less condensation. The weaker convection in AGCM/LSM is consistent with the reduced precipitation in central Amazonia shown in Fig. 4a. It is worth knowing that stronger interannual variability in convection is evident in AGCM/LSM since the standard deviation of Q_1 and Q_2 from AGCM/LSM are generally larger than that from AGCM/SLS.

Another evidence of convection intensity is given by the amount and distribution of upper tropospheric IWC. Ice clouds formation at the upper tropical troposphere by AGCMs is highly correlated with the moisture flux detrainment of cumulus convection. Regions with strong deep convection generally show high amount of IWC. The IWC from AGCM/SLS in central Amazonia is much larger than that in the observational estimates from the CloudSat (Fig. 6), which suggests that simulated convection is too strong locally. The values from AGCM/LSM compare better, which is consistent with more realistic convection strength. The center of maximum values, however, is slightly displaced to the west. These features are in agreement with those from the Q_1 and Q_2 analyses.

According to this analysis, upgrading the representation of land surface processes affects both near surface meteorological fields and the static stability of the entire atmospheric column over South America. Over central Amazonia, in particular, the more stable and drier atmosphere in AGCM/LSM results in weaker convection and precipitation. The causal link becomes established because

the cumulus parameterization in the AGCM is based on the quasi-equilibrium assumption, according to which convection intensity is determined by the convective available potential energy (CAPE) that depends on the static stability of the atmospheric column.

3.3 Impact on the low-level circulation

Figure 7 shows the December–February mean 850 mb velocity and wind speed from the ERA40 reanalysis (Fig. 7a) and the simulations (Fig. 7b, c). Overall, both simulations successfully capture the outstanding patterns in the reanalysis. Large-scale features, such as the intensity and distribution of equatorial trade winds and subtropical Atlantic high, are well represented in the model fields. The simulated northeasterly winds into the core region of SAMS around 10°S are slightly strong, however. Of high relevance to this study, a clear intensification of low level winds is found along the lee of Andes from 10°S to 20°S. As expected, the strong and mesoscale core of the SALLJ is missed due to insufficient model resolution. Nevertheless, the AGCM/LSM performance is clearly superior to AGCM/SLS in the SALLJ region.

We next look into the moisture transport in SALLJ region, which is crucial to the position and intensity of the SACZ (Marengo et al. 2004 and references there in), and to convection in the northwestern sector of La Plata Basin. Figure 8 shows a December–February mean vertical cross-section of meridional moisture flux at 20°S. At lower levels, the ERA40 Reanalysis shows two local enhancements of the northerlies; one is along the lee of the Andes and the other one is along the lee of the Brazilian Highlands. AGCM/SLS shows only one maximum west of the Brazilian Highlands, and unrealistic southerlies along the lee of the Andes. AGCM/LSM shows a much more realistic meridional moisture transport except for a slightly

Fig. 7 December–February mean 850 mb velocity and wind speed (m s^{-1}) for **a** ERA40 Reanalysis, **b** uncoupled UCLA AGCM with simple land scheme (AGCM/SLS), and **c** coupled UCLA AGCM-SSiB (AGCM/LSM). Also plotted in **d** the difference of December–February mean sea level pressure between AGCM/LSM and AGCM/SLS (contour is 1 mb), and regions where differences are statistically significant at the 95% confidence level are shaded
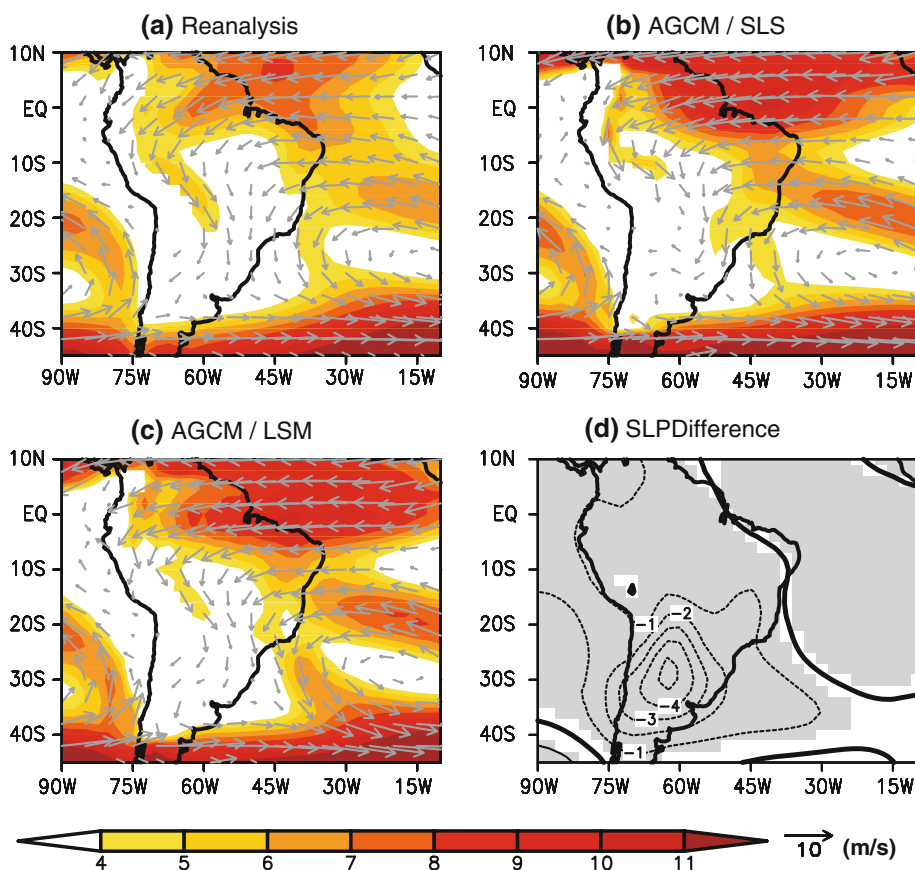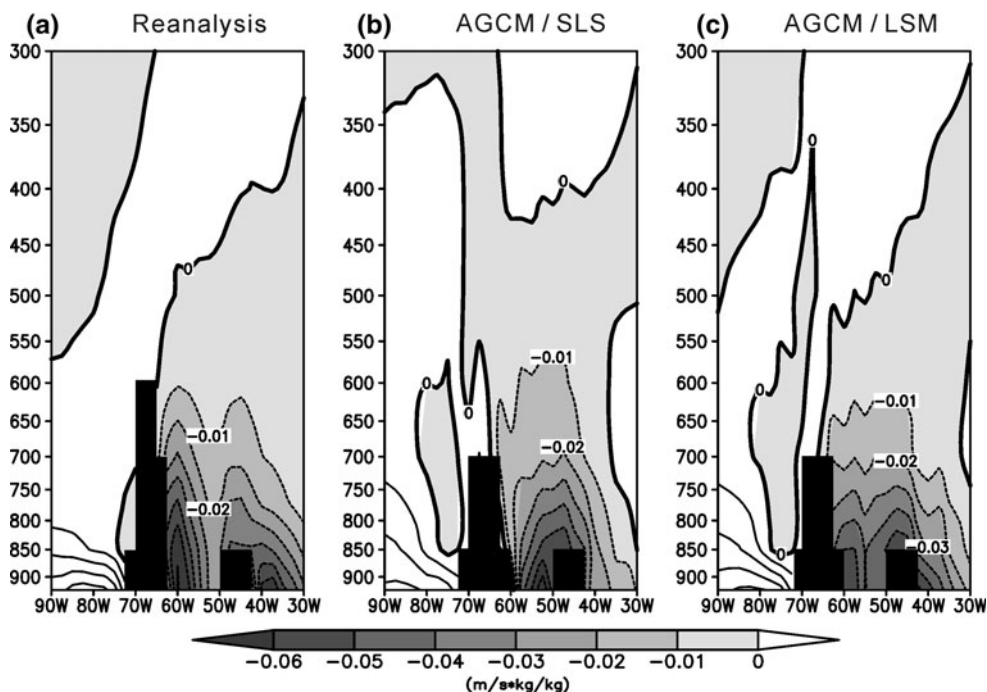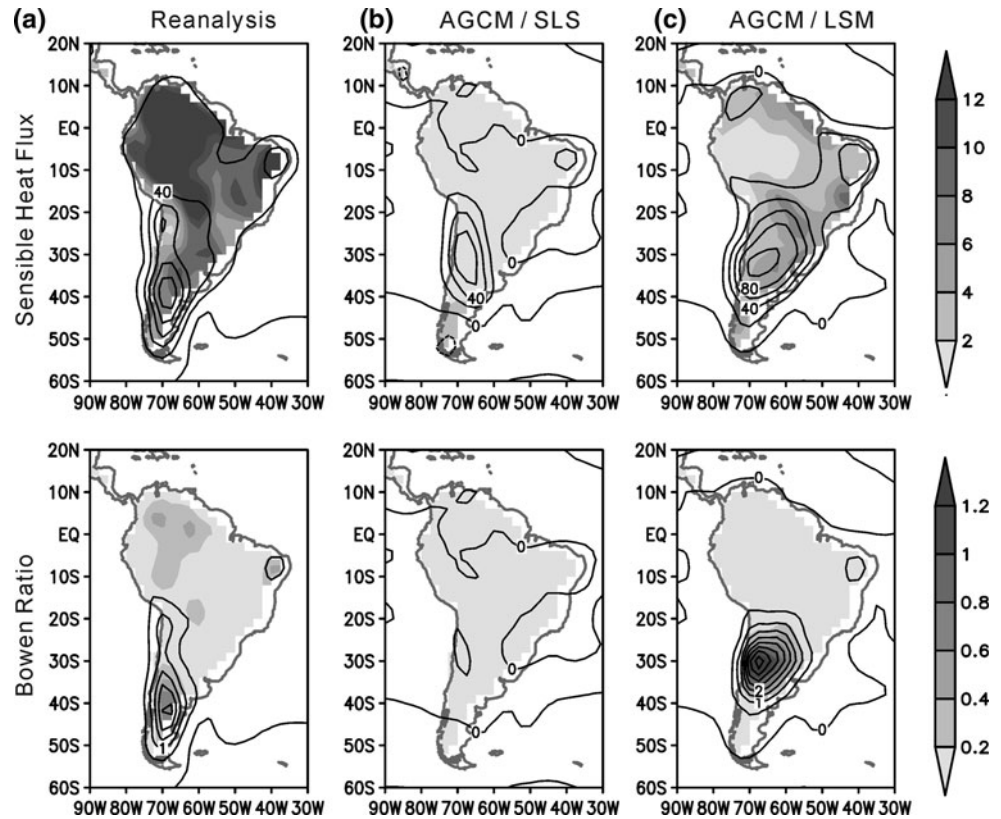

Fig. 8 Longitude-height (mb) sections of the December–February mean meridional moisture flux at 20°S from **a** ERA40 Reanalysis, **b** uncoupled UCLA AGCM with simple land scheme (AGCM/SLS), and **c** coupled UCLA AGCM-SSiB (AGCM/LSM). Contour interval is 0.01 (m s^{-1} kg kg^{-1}), and topography is shaded in *black*

weaker magnitude, consistently with the better simulation of low level winds in this region. The better SACZ intensity and position is consistent with the improvement of moisture transport in SALLJ region.

In order to investigate the reason for better representation of winds in SALLJ regions in the AGCM/LSM, we plot in Fig. 7d the difference of December–February mean SLP between AGCM/LSM and AGCM/SLS. The

Fig. 9 December–February mean surface sensible heat flux (W m^{-2}, *top* three), and the Bowen ratio (*bottom* three) from **a** ERA40 Reanalysis, **b** uncoupled UCLA AGCM with simple land scheme (AGCM/SLS), and **c** coupled UCLA AGCM-SSiB (AGCM/LSM). Contour is 20 (W m^{-2}) for sensible heat flux and 0.5 for Bowen ratio. Also plotted in *shade* is the standard deviation

difference field shows a local minimum on the lee of the Andes around 30°S. This region corresponds to the position of the Chaco Low, which is a thermal feature that develops over the central part of the continent during the southern summer. The Chaco Low is stronger in AGCM/LSM, which generates an anomalous cyclonic circulation at low levels. Consistently, the low-level flows at 850 mb, especially the northwesterlies on the lee of the Andes, are strengthened and become closer to those in the ERA40 Reanalysis.
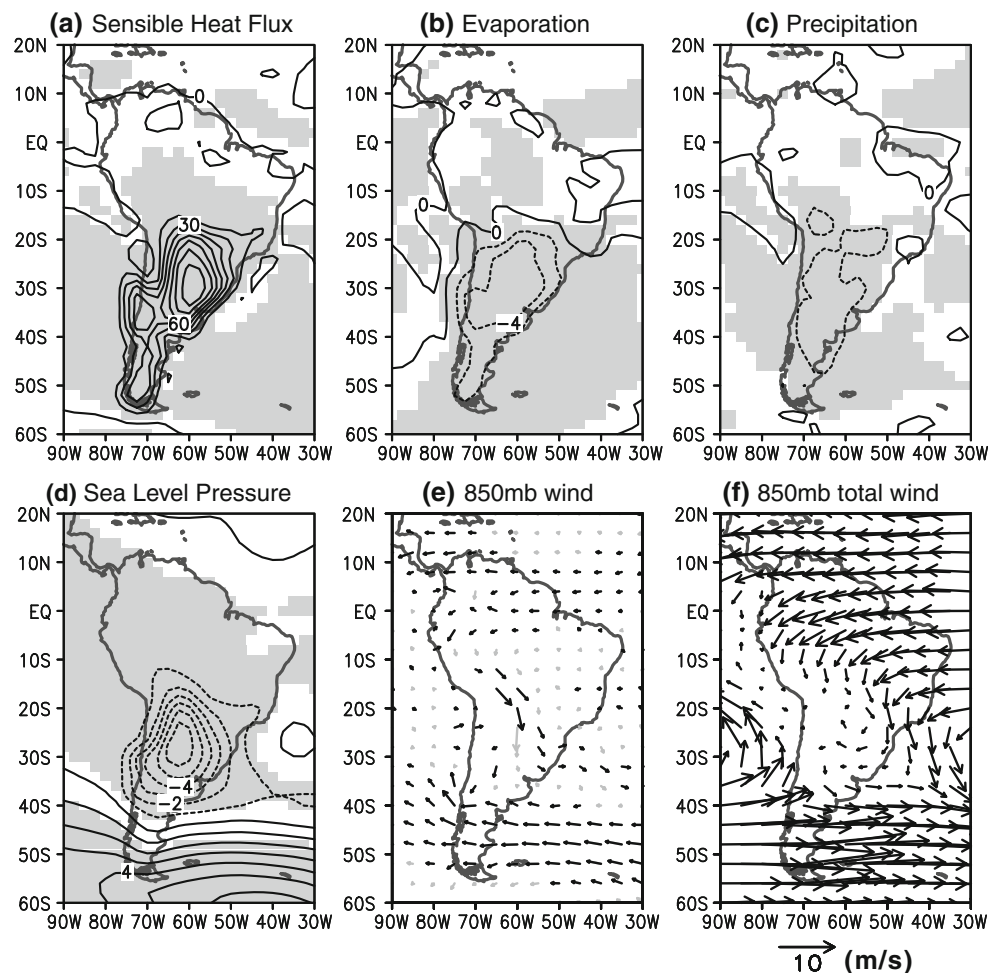
During the mature stage of SAMS, the Chaco Low develops mostly with the contribution of surface turbulent sensible heat flux (Zhou and Lau 1998). Figure 9 displays December–February mean surface sensible and Bowen ratio (contours) from the ERA40 Reanalysis and the simulations, as well as their standard deviation. Over South America, the reanalysis (Fig. 9a) shows a center of maximum sensible heat flux between 30°S and 40°S with 100 W m^{-2} in magnitude. AGCM/SLS (Fig. 9b) obtains a weaker value east of the Andes around 30°S; the reduction is at least 20 W m^{-2}. AGCM/LSM (Fig. 9c) performs significantly better and the corresponding values of Bowen ratio reveal a more realistic partition of sensible and latent heat fluxes than in AGCM/SLS. Therefore, upgrading the representation of land surface processes improves the simulated Chaco Low and low-level winds, sensible heat flux and Bowen ratio.

The standard deviation of sensible heat flux in Fig. 9, as in Fig. 5, also shows larger values and stronger interannual variability from AGCM/LSM than those from AGCM/SLS. The values either in AGCM/LSM or AGCM/SLS, however, are much smaller than that from ERA40, especially in the northern part of the South America. The larger signal of standard deviation in ERA40 can be explained as the influences of the interannual or decadal variability from both the atmosphere and ocean sides, while both AGCM experiments are performed with monthly-varying SST from the climatology.

4 On the mechanism of regional impact of land surface processes

The simulations described in Sect. 3 demonstrate that an upgrade in the representation of land surface processes in the AGCM results in an improved simulation of the warm season climate over South America. The analysis identifies two contributors to this success. First, improved surface heat fluxes in central Amazonia results in increased vertical stability of the atmospheric column, which reduces local precipitation to more realistic values. Second, a similar improvement in central South America results in a better intensity of Chaco Low and associated low-level wind system including the SALLJ region. In this section we

Fig. 10 Difference of
December–February mean **a**
surface sensible heat flux
(contour interval is 15 W m^{-2}),
b surface evaporation (contour
interval is 2 mm day^{-1}), **c**
precipitation (contour interval is
2 mm day^{-1}), **d** sea level
pressure (contour interval is
1 mb), and **e** 850 mb velocity
(m s^{-1}), between coupled
UCLA AGCM-SSiB (AGCM/
LSM) and coupled UCLA
AGCM-SSiB except the simple
land scheme is used in the
region of poleward of 20°S in
the South America (AGCM/
SOUTH20S). Regions in **a**–**d**,
and *vectors* in **e** where
differences are statistically
significant at the 95%
confidence level are *shaded*, and
in *dark black*, respectively. Also
plotted in **f** the December–
February mean 850 mb velocity
(m s^{-1}) from AGCM/
SOUTH20S

examine whether these two contributors act either independently or interact with each other.

Our approach is based on performing two idealized experiments. First, the AGCM is coupled to SSiB globally except in South America *poleward* of 20°S, where the simple land surface scheme is used. In this experiment, which we will refer to as AGCM/SOUTH20S, surface fluxes are degraded in locations that include that of the Chaco Low. In the second idealized experiment, the AGCM coupling to SSiB is performed everywhere, except over South America *equatorward* of 20°S. In this experiment, which we refer to as AGCM/NORTH20S, surface fluxes are degraded in central Amazonia. Both experiments are five-years long and use prescribed, time-varying, monthly mean SSTs from an observed climatology (Reynolds and Smith 1995). The descriptions in this section are made taking the AGCM/LSM fields as reference.

The results from the first idealized experiment are fairly straightforward to interpret. Figure 10 presents differences between AGCM/LSM and AGCM/SOUTH20S (SSiB everywhere except over South America poleward of 20°S). The magnitudes are small outside the region where the

treatment of land surface processes is degraded. It is apparent that the enhanced Chaco Low (Fig. 10d) is associated with local enhancements of surface heat flux (Fig. 10a), which are due to the different effects of local land surface processes. The northwesterlies in the SALLJ region are improved, but winds further north in central Amazonia (Fig. 10e) are hardly modified. The distribution of 850 mb velocity on the lee of the Andes from AGCM/SOUTH20S shows weaker northwesterlies, and unrealistic southerlies are even present around 20°S–30°S. The results of this idealized experiment, therefore, suggest that the improvement in the intensity of Chaco Low and associated low-level flows are controlled by local effects of land surface processes.

Interpreting the results from the second idealized experiments require more elaboration. Figure 11 shows the differences between AGCM/LSM (SSiB everywhere) and AGCM/NORTH20S (no SSiB in South America equatorward of 20°S) in surface sensible and latent heat fluxes (Fig. 11a, b, respectively), precipitation (Fig 11c), and velocity at the 850 mb level (Fig. 11d). The magnitudes in the panels of Fig. 11 are larger north of 20°S. In this
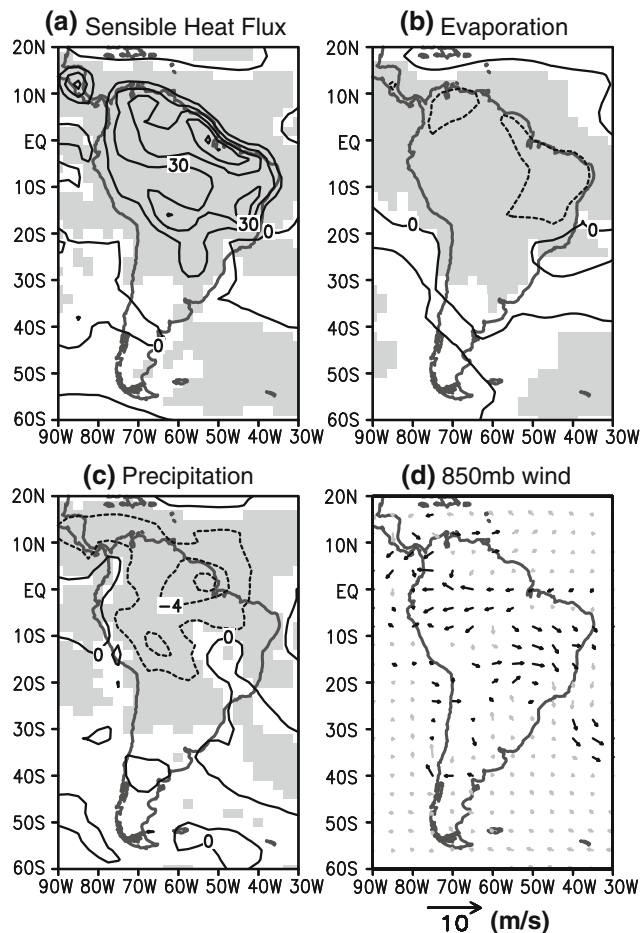
Fig. 11 Difference of December–February mean **a** surface sensible heat flux (contour interval is 15 W m^{-2}), **b** surface evaporation (contour interval is 2 mm day^{-1}), **c** precipitation (contour interval is 2 mm day^{-1}), and **d** 850 mb velocity (m s^{-1}), between coupled UCLA AGCM-SSiB (AGCM/LSM) and coupled UCLA AGCM-SSiB except the simple land scheme is used in the region of equatorward of 20°S in the South America (AGCM/NORTH20S). Regions in **a–c**, and *vectors* in **d** where differences are statistically significant at the 95% confidence level are *shaded*, and in *dark black*, respectively

region, sensible heat flux decreases and evaporation slightly increases in AGCM/NORTH20S. The precipitation increases in central Amazonia, as the static stability of the atmosphere decreases. The situation is different in the SACZ region, where precipitation increases slightly. The magnitudes of the differences in sensible and latent heat fluxes and in moisture flux convergence south of 20°S are generally small. The small differences in 850 mb winds south of 20°S indicate that land surface processes equatorward of that latitude have little impact on the low-level flows in central South America. The differences of precipitation in central Amazonia in the panels of Fig. 11c are about one-half those between AGCM/LSM and AGCM/SLS (Fig. 4). It appears, therefore, that the differences over tropical South America between AGCM/LSM and AGCM/SLS cannot be interpreted solely in terms of local changes of static stability in the atmospheric column.

Recycled precipitation in the Amazon is important and the amount can account for 25% of observed precipitation (Eltahir and Bras 1994). Nevertheless, the source of moisture for convection in tropical South America is mainly provided by the trade winds, which bring moist air from tropical Atlantic Ocean. Part of the moisture in the Amazon basin is then transported southeastward toward the SACZ region and La Plata Basin. We plot in Fig. 12 the December–February mean of vertically integrated moisture flux from AGCM/SLS and AGCM/NORTH20S, as well as their differences. Both AGCM/SLS (Fig. 12a) and AGCM/NORTH20S (Fig. 12b) capture the overall pattern. There are, however, differences between the two simulations (Fig. 12c). Figure 12c shows that moisture convergence in the core of SAMS is stronger in AGCM/SLS than in AGCM/NORTH20S. The stronger precipitation and moisture flux convergence in AGCM/SLS could be explained by the stronger positive feedback between the two processes. There is also a hint of less moisture transport around 20°S–30°S in the SALLJ regions in AGCM/SLS since the AGCM/NORTH20S has better low-levels flows on the lee of the Andes around 20°S–30°S due to the local effect of land surface processes, evidenced in AGCM/SOUTH20S. Therefore, the precipitation difference between AGCM/SLS and AGCM/LSM in tropical South America must be attributed to both changes in static stability of the atmospheric column due to local changes in land surface processes, and to changes in large-scale moisture convergence due to changes in the large-scale flow (trades) and the regional flow in the Chaco Low region.

This analysis suggests that the improved simulation of the warm season climate over South America requires a better representation of surface processes over the entire continent. Although a higher success is desirable in the monsoon region in view of the teleconnections with other climate features such as the subtropical highs (e.g., Rodwell and Hoskins 2001), the full potential improvement requires consideration of the subtropics.

5 Summary and conclusions

The distributions of continental masses, orography and SSTs combine to define the characteristics of the SAMS, which is a key feature of South America in the warm season climate. The summertime upper-level anticyclone/low-level heat low that characterizes a monsoon circulation is in spatial quadrature in longitude with ascent on the eastern side and subsidence on the western side (Chen 2003). This configuration of phase allows for a largely
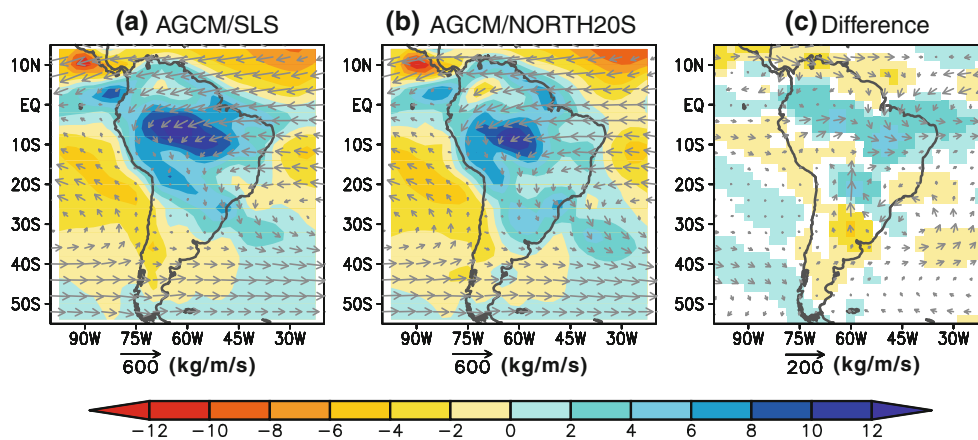
Fig. 12 December–February mean of vertically integrated moisture flux (*vector*, kg m^{-1} s^{-1}) and its convergence (*shaded*, mm day^{-1}) from **a** uncoupled UCLA AGCM (AGCM/SLS), and coupled UCLA AGCM-SSiB except the simple land scheme is used in the region of equatorward of 20°S in the South America (AGCM/NORTH20S). Also plotted in **c** the difference between (**a**–**b**), and only the values of convergence that are statistically significant at the 95% confidence level are *shaded*

Sverdrup-type balance between the vorticity source associated with diabatically forced continental-scale vertical motion, and advection of planetary vorticity. The low-level poleward motion associated with the Sverdrup balance feeds warm moist air into the convective regions in a positive feedback. The SAMS comprises convection over Amazonia and the SACZ; along the eastern scarp of the Andes, where the SALLJ develops with strongest winds over Bolivia. The SALLJ transports considerable moisture between the Amazon and La Plata basins and is present throughout the year (e.g., Berbery and Barros 2002; Byerle and Paegle 2002; Campetella and Vera 2002). It has been suggested that AGCM difficulties with this mesoscale feature are a major impediment to the successful simulation of the SAMS. According to this suggestion, very high model resolutions would be required to overcome such impediment. The present paper does not challenge the notion that the mesoscale features of the SALLJ and associated development of mesoscale convective systems—the strongest in the world. However, we demonstrate that upgrading land surface processes in an AGCM to include representation of both soil and vegetation processes produces a major improvement in the simulated climatology of surface fluxes, low-level circulations, and precipitation that define SAMS. We also examine how these improvements are achieved.

Our conclusion is based on comparison between two 30-year long experiments of the UCLA AGCM using either a very simple land scheme (AGCM/SLS) or coupled to a much more comprehensive representation of land surface processes provided by SSiB (AGCM/LSM). The comparison concentrates on the South American continent during the warm season. In this section of the paper and for easiness of presentation we will refer to AGCM/SLS as the "uncoupled case" and to AGCM/LSM as the "coupled case".

In the coupled case, the surface sensible heat flux generally increases and the surface latent heat flux (or evaporation) generally decreases over South America in reference to the uncoupled case. This represents an improvement since simulated fields in the coupled case are closer to the ERA40 Reanalysis. The Bowen ratio, which is the ratio of sensible heat flux to latent heat flux, is also improved.

In addition, the low-level wind distribution is improved in the coupled case, especially along the lee side of the Andes in the SALLJ region. The SACZ is also improved, consistently with the better transport of moisture flux in the SALLJ region. Based on the experiments with the globally coupled AGCM, and the same coupled AGCM except for the region of South America *poleward* of 20°S—where it is uncoupled—the results suggest that the improvement of the large scale flows are consistent with the better intensity of the Chaco Low, which is associated with better simulated surface sensible heat flux in the southern South America.

The coupled case produces more realistic precipitation amounts in central Amazonia than the uncoupled case, in which values are higher. The reduction is due to decreased convection as indicated by the analyses of large-scale heat and moisture budget residuals represented by apparent heat source Q_1 and moisture sink Q_2, as well as by the cloud IWC in the upper troposphere. The heating profile from AGCM uncoupled shows stronger heating at mid-tropospheric levels in central Amazonia, while that from AGCM coupled is closer to estimates from ERA40. The experiments with the globally coupled AGCM, and the same coupled AGCM except for the region of South America *equatorward* of 20°S where it is uncoupled, indicate that

the mechanisms for improvement of precipitation are complex and not necessarily local. Almost one-half of the precipitation difference between AGCM/SLS and AGCM/LSM in tropical South America are attributed to the changes in the atmospheric column static stability due to the changes of local land surface processes. The other half of the difference is attributed to changes in the large-scale moisture convergence. The reasons for this are due to less intense positive feedback between precipitation, and moisture convergence, as well as more moisture source been transported out of the core of monsoon regions.

With the advanced land surface model incorporated in the AGCM, both the surface heat flux (Fig. 9) and the convection (Fig. 5) show larger interannual variability in the coupled case. This suggests the land surface processes can not only affect the mean climatology of the atmosphere but also the intensity of interannual or even longer time scale variability.

It is difficult to draw an analogy between our findings and those of Collini et al. (2008). First, our experiments are performed in a climate mode while those of Collini et al. (2008) examine an initial value problem. Second, although SSiB recognizes soil moisture explicitly, the simple land surface scheme only does it indirectly through the prescribed potential evapotranspiration. Third, our changes are variable in space, while theirs are spatially uniform. Nevertheless we could attempt a parallel on the basis of the sensible heat fluxes. Collini et al. (2008) obtain increased surface sensible heat fluxes and decreased latent fluxes as a result of negative initial perturbations in soil moisture; we obtain differences of the same sign between the coupled and uncoupled cases. In both cases, the warmer and drier atmosphere is interpreted as reducing the atmospheric instability. Therefore, our findings suggest a caveat in the interpretation of regions with strong coupling between soil moisture and precipitation (Koster et al. 2004) as indicators of where land surface processes have strong impacts on the circulation. Koster et al. (2004) identify central Amazonia as a "hot spot" in reference to the regions where soil moisture anomalies have substantial impact on precipitation during the northern summer. Our results confirm the "hot spot" labeling of that region for the southern summer, and suggest that a region with different characteristics (Chaco Low) can also provide important contribution to the circulation. Contemporaneous AGCMs use parameterization of land surface processes that are closer to SSiB than to the simple land surface models. The results of idealized experiments such as those presented here would help to evaluate model performance.

References

Arakawa A (2000) A personal perspective of the early years of general circulation modeling at UCLA. In: Randall DA (ed) General circulation model development: past, present, and future. Proceedings of a symposium in Honor of Professor Akio Arakawa. Academic Press, pp 1–65

Arakawa A, Schubert WH (1974) Interaction of a cumulus ensemble with the large-scale environment. Part I. J Atmos Sci 31:674–701

Beljaars ACM, Viterbo P, Miller MJ, Betts AK (1996) The anomalous rainfall over the United States during July 1993: sensitivity to land surface parameterization and soil moisture anomalies. Mon Wea Rev 124:362–383

Berbery EH, Barros VR (2002) The hydrologic cycle of the La Plata Basin in South America. J Hydrometeor 3:630–645

Betts AK, Ball AJ, Viterbo P, Dai A, Marengo J (2005) Hydrometeorology of the Amazon in ERA-40. J Hydrometeor 6:764–774

Bombardi RJ, Carvalho LMV (2009) IPCC global coupled model simulations of the South America monsoon system. Clim Dyn 33. doi:10.1007/s00382-008-0488-1

Businger JA, Wyngaard JC, Izumi Y, Bradley EG (1971) Flux–profile relationships in the atmospheric surface layer. J Atmos Sci 28:181–189

Byerle LA, Paegle J (2002) Description of the seasonal cycle of low-level flows flanking the Andes and their interannual variability. Meteorologica 27:71–88

Campetella CM, Vera CS (2002) The influence of the Andes mountains on the South American low-level flow. Geophys Res Lett 29. doi:10.1029/2002GL015451

Chen T-C (2003) Maintenance of summer monsoon circulations: a planetary scale perspective. J Clim 16:2022–20037

Collini EA, Berbery EH, Barros VR, Pyle ME (2008) How does soil moisture influence the early stages of the South American monsoon? J Clim 21:195–213

Deardorff JW (1972) Parameterization of the planetary boundary layer for use in general circulation models. Mon Wea Rev 100:93–106

Dirmeyer PA, Koster RD, Guo Z (2006) Do global models properly represent the feedback between land and atmosphere? J Hydrometeor 7:1177–1198

Dirmeyer PA, Schlosser CA, Brubaker KL (2009) Precipitation, recycling, and land memory: an integrated analysis. J Hydrometeor 7:1177–1198

Dorman JL, Sellers PJ (1989) A global climatology of albedo, roughness length and stomatal resistance for atmospheric general circulation models as represented by the Simple Biosphere Model (SiB). J Appl Meteor 28:833–855

Eltahir EAB, Bras RL (1994) Precipitation recycling in the Amazon basin. Quart J R Meteor Soc 120:861–922

Fernandes K, Fu R, Betts AK (2008) How well does the ERA40 surface water budget compare to observations in the Amazon River basin? J Geophys Res. doi:10.1029/2007JD009220

Grimm AM, Pal JS, Giorgi F (2007) Connection between spring conditions and peak summer monsoon rainfall in South America:

role of soil moisture, surface temperature, and topography in Eastern Brazil. J Clim 20:5929–5945

Harshvardhan, Davies R, Randall DA, Corsetti TG (1987) A fast radiation parameterization for atmospheric circulation models. J Geophys Res 92:1009–1016

Harshvardhan, Davies R, Randall DA, Corsetti TG, Dazlich DA (1989) Earth radiation budget and cloudiness simulations with a general circulation model. J Atmos Sci 46:1922–1942

Hung C-W (2003) Variabilities of the Asian–Australian monsoon system from annual to interdecadal timescales. PhD. Dissertation, Department of Atmospheric Sciences, University of California, Los Angeles

Intergovernmental Panel on Climate Change (2007) Climate change 2007: the physical science basis. Cambridge University Press, Cambridge

Kodama Y-M (1992) Large-scale common features of subtropical precipitation zones (the Baiu Frontal Zone, the SPCZ, and the SACZ). Part I: characteristics of subtropical frontal zones. J Meteor Soc Jpn 70:813–835

Köhler M (1999) Explicit prediction of ice clouds in general circulation models. Ph.D. Dissertation, Department of Atmospheric Sciences, University of California, Los Angeles

Koster RD et al (2004) Regions of coupling between soil moisture and precipitation. Science 305:1138–1140

Kummerow C et al (2000) The status of the tropical rainfall measuring mission (TRMM) after two years in orbit. J Appl Meteor 39:1965–1982

Lenters JD, Cook KH (1995) Simulation and diagnosis of the regional summertime precipitation climatology of South America. J Clim 8:2988–3005

Li J-L, Köhler M, Farrara JD, Mechoso CR (2002) The impact of stratocumulus cloud radiative properties on surface heat fluxes simulated with a general circulation model. Mon Wea Rev 130:1433–1441

Liebmann B, Allured D (2005) Daily precipitation grids for South America. Bull Am Meteor Soc 86:1567–1570

Lin J-L, Qian T, Shinoda T, Liebmann B, Zheng Y, Han W, Roundy P, Zhou J (2009) Intraseasonal variability associated with summer precipitation over South America simulated by 14 WRCP CMIP3 coupled GCMs. Mon Wea Rev 137:2931–2954

Luo H, Yanai M (1984) The large-scale circulation and heat sources over the Tibetan Plateau and surrounding areas during the early summer of 1979. Part II: heat and moisture budgets. Mon Wea Rev 112:130–141

Marengo JA et al (2003) Assessment of regional seasonal rainfall predictability using the CPTEC/COLA atmospheric GCM. Clim Dyn 21:459–475

Marengo JA, Soares WR, Saulo C, Nicolini M (2004) Climatology of the low-level jet east of the Andes as derived from the NCEP–NCAR reanalyses: characteristics and temporal variability. J Clim 15:2261–2280

Mechoso CR, Yu JY, Arakawa A (2000) A coupled GCM pilgrimage: From climate catastrophe to ENSO simulations. In: Randall DA (ed) General circulation model development: past, present, and future. Proceedings of a symposium in Honor of Professor Akio Arakawa. Academic Press, pp 539–575

Mechoso CR, Robertson AW, Ropelewski CF, Grimm AM (2004) The American Monsoon Systems. In: Proceeding of the 3rd international workshop on monsoons. Hangzhou, China, November, pp 2–6

Meehl GA, Arblaster JM, Lawrence DM, Seth A, Schneider EK, Kirtman BP, Min D (2006) Monsoon regimes in the CCSM3. J Clim 19:2482–2495

Mintz M (1984) The sensitivity of numerically simulated climates to land-surface boundary conditions. In: Houghton JT (ed) The global climate. Cambridge University Press, UK, pp 79–105

Nogués–Paegle J, Mechoso CR, Fu R et al (2002) Progress in pan American CLIVAR research: understanding the South American monsoon. Meteorologica 27:1–30

Pal JS, Eltahir EAB (2001) Pathways relating soil moisture conditions to future summer rainfall within a model of the land-atmosphere system. J Clim 14:1227–1242

Pan D-M, Randall DA (1998) A cumulus parameterization with a prognostic closure. Quart J R Meteorol Soc 124:949–981

Paulson CA (1970) Mathematical representation of wind speed and temperature profiles in the unstable atmospheric surface layer. J Appl Meteor 9:857–861

Reynolds RW, Smith TM (1995) A high-resolution global sea surface temperature climatology. J Clim 8:1571–1583

Rodwell MJ, Hoskins BJ (2001) Subtropical anticyclones and summer monsoons. J Clim 14:3192–3211

Sellers PJ, Mintz Y, Sud YC, Dalcher A (1986) A simple biosphere model (SiB) for use within general circulation models. J Atmos Sci 43:505–531

Suarez MJ, Arakawa A, Randall DA (1983) The parameterization of the planetary boundary layer in the UCLA general circulation model: formulation and results. Mon Wea Rev 111:2224–2243

Stephens GL et al (2008) CloudSat mission: performance and early science after the first year of operation. J Geophys Res. doi:10.1029/2008JD009982

Uppala SM et al (2005) The ERA-40 re-analysis. Quart J R Meteorol Soc 131:2961–3012

Vera C et al (2006a) Toward a unified view of the American monsoon systems. J Clim 19:4977–5000

Vera C, Silvestri G, Liebmann B, González P (2006b) Climate change scenarios for seasonal precipitation in South America from IPCC-AR4 models. Geophys Res Lett. doi:10.1029/2006GL025759

Waliser DE, Li J-LF, Woods CP et al (2009) Cloud ice: a climate model challenge with signs and expectations of progress. J Geophys Res. doi:10.1029/2008JD010015

Woods CP, Waliser DE, Li J-L, Austin RT, Stephens GL, Vane DG (2008) Evaluating CloudSat ice water content retrievals using a cloud-resolving model: sensitivities to frozen particle properties. J Geophys Res. doi:10.1029/2008JD009941

Xie P, Arkin PA (1997) Global precipitation: a 17-year monthly analysis based on gauge observations, satellite estimates, and numerical model outputs. Bull Am Meteor Soc 78:2539–2558

Xue Y, Sellers PJ, Kinter JL III, Shukla J (1991) A simplified biosphere model for global climate studies. J Clim 4:345–364

Xue Y, Bastable HG, Dirmeyer PA, Sellers PJ (1996a) Sensitivity of simulated surface fluxes to changes in land surface parameterization—a study using ABRACOS data. J Appl Meteor 35:386–400

Xue Y, Fennessy MJ, Sellers PJ (1996b) Impact of vegetation properties on US summer weather prediction. J Geophys Res 101:7419–7430

Xue Y, De Sales F, Li W, Mechoso CR, Nobre C, Juang H-MH (2006) Role of land surface processes in South American monsoon development. J Clim 19:741–762

Xue Y, De Sales F, Vasic R, Mechoso CR, Arakawa A, Prince S (2010) Global and seasonal assessment of interactions between climate and vegetation biophysical processes: a GCM study with different land–vegetation representations. J Clim 23:1411–1433

Yanai M, Tomita T (1998) Seasonal and interannual variability of atmospheric heat sources and moisture sinks as determined from NCEP–NCAR reanalysis. J Clim 11:463–482

Yanai M, Esbensen S, Chu J–H (1973) Determination of bulk properties of tropical cloud clusters from large-scale heat and moisture budgets. J Atmos Sci 30:611–627

Zeng N, Neelin JD (1999) A land-atmosphere interaction theory for the tropical deforestation. J Clim 12:857–872

Zhou J, Lau WK–M (1998) Does a monsoon climate exist over South America. J Clim 11:1020–1040

Zhou J, Lau WK-M (2002) Intercomparison of model simulations of the impact of 1997/98 El Niño on South American summer monsoon. Meteorologica 27:99–116